Noise and Vibration: *Emerging Methods*
**NOVEM 2009**
5-8 April 2009 Oxford

# STRUCTURE-BORNE SOUND IN FLAT PLATES EXCITED BY TURBULENT BOUNDARY LAYERS

Stephen Hambric[1] and Michael Daley[2]

[1]Applied Research Lab
Penn State University, PO Box 30, State College, Pennsylvania, 16804, USA
Email: sah19@only.arl.psu.edu

[2]Akustica, Inc.
2835 East Carson Street, Suite 301, Pittsburgh, Pennsylvania, 15203, USA
Email: mdaley@akustica.com

## ABSTRACT

*An analytical model of the structure-borne sound within flat plates excited by spatially random pressure fields is described. The model, validated previously using measurements of the structural intensity in a rectangular plate driven by a diffuse sound field, is exercised using turbulent boundary layer (TBL) wall pressures. TBL pressure fields are applied to a flat plate at various flow speeds, and power input and structural intensity are computed at the resonance frequencies of several modes. At low flow speeds, when the convection speed of the TBL wall pressures is slower than or comparable to the plate bending wave speed, the structural intensity fields in the plate do not vary significantly with flow speed. At very high flow speeds, the intensity patterns change, and eventually converge to the patterns caused by fully correlated, non-spatially varying pressure loads. Although the structural intensity patterns do not change significantly over most flow speeds of practical interest, the total power injected into the plate varies substantially with flow speed, peaking near, but not necessarily at, the coincidence of the plate bending and flow convective wavespeeds.*

## 1 INTRODUCTION

Structural intensity (S-I) fields indicate the magnitude and direction of energy flow through a vibrating structure as a function of position. Various experimental and computational studies have been performed for simple plate and beam structures excited deterministically at a point or group of points [1-9]. Thus far, insufficient attention has been paid to intensity fields in structures excited by distributed, random, fluctuating pressure fields, such as those due to turbulent boundary layers or diffuse acoustic excitation. In randomly excited structures, the fluctuating velocity and stress fields are only partially correlated over space. For example, the turbulent eddies within a boundary layer over an aircraft wing or propeller blade (like the one shown in Figure 1) are coherent only over small regions. The turbulence near a wing tip, for example, is completely incoherent with the turbulence near the joint with the fuselage.

The aerospace, automotive, nuclear, and naval communities have developed multiple-input/multiple output techniques for analyzing the vibrations and strains within structures

excited by partially coherent excitation fields [10-18]. However, little attention has been given to the structural intensity fields in randomly excited structures.

Figure 1 shows notional structural intensity patterns in a propeller blade and hub, caused by spatially random pressures acting on one of the blades. While computational methods like FE analysis [3, 4] may be used to compute intensity fields like these given a deterministic point drive (or set of point drives), there are no techniques available to simulate intensities induced by spatially random pressure fields.

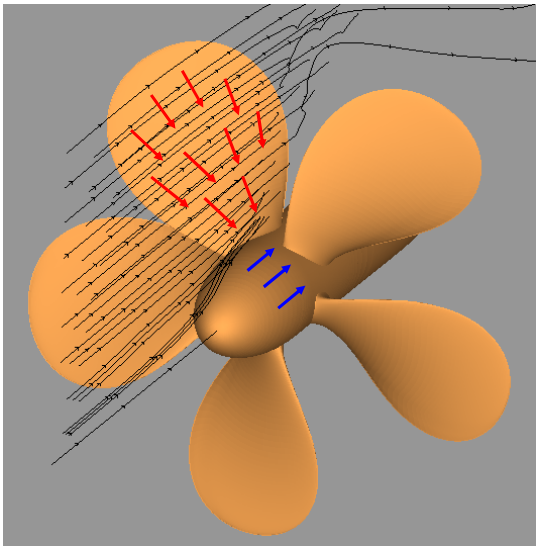

Figure 1: Example of notional structural intensity field on the blade of a propeller excited by a convecting turbulent pressure field, along with intensities on the shaft.

Daley and Hambric presented previously an analytic method of simulating structural intensity fields in structures excited by distributed random pressure fields [19]. The approach, based on combining transfer function matrices between structural forces and displacements with cross-spectral density functions of spatially random applied forces, has been validated against simulations made using the well known finite differencing approach for flat rectangular plates excited by spatially random diffuse acoustic fields, and against measurements [19, 20].

The method is used here to investigate how the structure-borne sound in plates is affected by the fluctuating wall pressures induced by turbulent boundary layer (TBL) flow fields, and in particular how the TBL flow velocity affects structural intensities. It is well known that TBL wall pressures are dominated by contributions at the convective wavenumber ($\omega/U_c$, where $U_c$ is the effective convection velocity of the TBL wall pressures propagating over the surface). When the convective wavenumber coincides with wavenumber peaks of structural vibration, significant response occurs. However, when the convective and peak structural wavenumbers are misaligned, plate vibration (and structural intensities) are small. In this study, TBL pressure fields are applied to a flat rectangular baffled plate at various flow speeds, and power input and structural intensity are computed at the resonance frequencies of low-order modes. The behaviour of the power input and intensity fields as a function of flow velocity is described and explained.

## 2 SUMMARY OF METHODOLOGY

Throughout this article the term "intensity" is used to describe the active part of the total intensity, or the in-phase portion of the potential and flow variable pairs of the intensity components. In thin plates undergoing flexural vibration, the total active structural intensity vectors consist of components due to shear waves, bending waves and twisting waves. Following the conventions of references [9] and [20], the orthogonal components of intensity may be written as:

$$I_x = \frac{\langle Q_x \dot{w} \rangle_t + \langle M_x \dot{\theta}_y \rangle_t - \langle M_{xy} \dot{\theta}_x \rangle_t}{h} = I_x^s + I_x^b + I_x^t \tag{1}$$

$$I_y = \frac{\langle Q_y \dot{w} \rangle_t - \langle M_y \dot{\theta}_x \rangle_t + \langle M_{xy} \dot{\theta}_y \rangle_t}{h} = I_y^s + I_y^b + I_y^t \tag{2}$$

where $Q$ is shear force/length, $M$ is moment/length, $w$ is transverse displacement, $\theta$ is rotation about the plate's neutral axis, $h$ is the plate thickness, and the 'dots' indicate time derivatives. The superscripts, $s$, $b$, and $t$, on the right sides of the preceding equations denote shear, bending and twisting components, respectively. Figure 2 is a free body diagram of a differential element of a plate showing the assumed orientations of the vector quantities contained in Equations (1-2). The total S-I vectors are the vector sums of Equations (1-2):

$$\bar{I} = I_x \hat{i} + I_y \hat{j} \,. \tag{3}$$

Suppressing the frequency dependence, one may rewrite Equations (1) and (2) in terms of cross spectra [19, 21, 22]:

$$I_x = \frac{1}{h} \Re \left\{ G_{q_x \dot{w}} + G_{m_x \dot{\theta}_y} - G_{m_{xy} \dot{\theta}_x} \right\}, \text{ and} \tag{4a}$$

$$I_y = \frac{1}{h} \Re \left\{ G_{q_y \dot{w}} - G_{m_y \dot{\theta}_x} + G_{m_{xy} \dot{\theta}_y} \right\}. \tag{4b}$$

As shown in [19], the cross spectra terms in equation (4) may be computed using :

$$G_{q_x \dot{w}} = H^H_{pq_x} G_{pp} H_{p\dot{w}}\,,\; G_{m_x \dot{\theta}_y} = H^H_{pm_x} G_{pp} H_{p\dot{\theta}_y}\,, \text{ and } G_{m_{xy} \dot{\theta}_x} = H^H_{pm_{xy}} G_{pp} H_{p\dot{\theta}_x} \text{ ; and} \tag{5a}$$

$$G_{q_y \dot{w}} = H^H_{pq_y} G_{pp} H_{p\dot{w}}\,,\; G_{m_y \dot{\theta}_x} = H^H_{pm_y} G_{pp} H_{p\dot{\theta}_x}\,, \text{ and } G_{m_{xy} \dot{\theta}_y} = H^H_{pm_{xy}} G_{pp} H_{p\dot{\theta}_y}\,. \tag{5b}$$

The $H$ matrices contain transfer functions between the inputs (pressures) and outputs (displacements, rotations, shears, and moments), and may be computed analytically for simple flat plates, or using Finite Element (FE) analysis for more complicated structures. Note that no finite differencing assumptions are made in the above formulation.

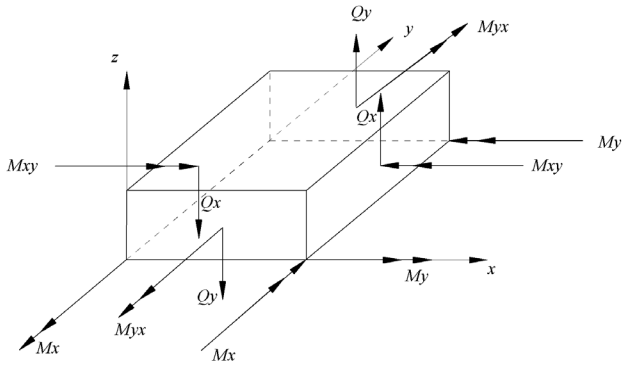


Figure 2: Free body diagram of differential element of plate.

## 3 TEST CASE

The structural intensity methods are applied to a baffled, thin rectangular plate, simply-supported on all four sides, excited by a turbulent boundary layer flow, as shown in Figure 3. The plate dimensions are 11.2 cm (*x* direction) by 7.5 cm (*y* direction) by 0.3175 cm thick. It is composed of Brass 260 (a.k.a. Cartridge Brass), a readily available material. The material properties of Brass 260 are Young's modulus: $E = 11.0 \times 10^{10}$ Pa, Poisson's ratio: $\nu$ = 0.375 and density: $\rho = 8525$ kg/m$^3$. The material loss factor used in the simulations was estimated previously from experiment as $\eta$= 0.002. A point damper with mechanical resistance $R_m = 40$ N·s/m and a moving mass $m_R = 1$ gram is located in the upper right quadrant of the plate at (8.80,5.25) cm.

Because the plate is thin and simply-supported, the frequency response matrices (*H*) used in the simulations may be obtained analytically by a summation of the plate's normal modes [19]. Responses were computed over a grid of points on the plate, chosen to resolve spatially the wavelengths of flexural waves and the turbulent boundary layer wall pressure field exciting the surface (a guideline of eight grid points per wavelength was followed). In this case, all points in the grid are excited by the pressure field, and intensities are computed for all grid points. The pressure response matrices are relatively simple to compute, since the plate is simply supported on all four sides and, for lower order modes, fits the criterion for thin plate calculations (i.e., $k_b h < 1$, where $k_b$ is the bending wavenumber of a mode).

The applied pressure model is that of a turbulent boundary layer wall pressure field, where the cross-spectra between pressures at two points, *i* and *j* may be approximated using the well known model of Corcos [23]:

$$\frac{G_{p_i p_j}(\omega, \Delta x, \Delta y)}{\mathbf{\Phi}_{pp}(\omega)} = \left( e^{-\omega \alpha_x |\Delta x|/U_c} e^{-\omega \alpha_y |\Delta y|/U_c} \right) e^{i\omega \Delta x/U_c}, \qquad (6)$$

where $\Delta x$ and $\Delta y$ are the separation distances between points on the plate, $\alpha_x$ and $\alpha_y$ are the decay coefficients of the wall pressure fluctuations in the streamwise (*x*) and cross-flow (*y*) directions (chosen to be 0.1 and 0.77 for smooth walls), and $U_c$ is the convective velocity, usually about 70% of the free stream velocity. The pressure cross spectrum is normalized by the wall pressure autospectrum $\mathbf{\Phi}_{pp}$, so that this study focuses on the effects of the cross-spectral behavior of the TBL field on the plate intensities. The term in ( ) in Equation 6 represents a spatial decay of the wall pressures, and the term following the ( ) is an oscillating wave propagating in the flow direction. While it is well known that the Corcos model overestimates the low-wavenumber components of the wall pressure field [24], it is suitable for analyzing trends in plate structural intensities as a function of flow (and convection) velocity.

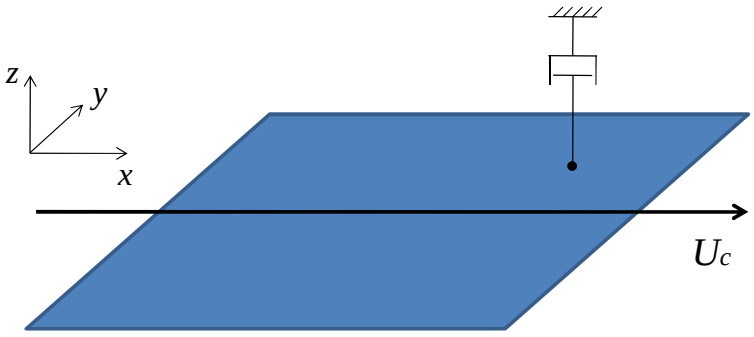


Figure 3: Simply supported rectangular flat plate excited by TBL flow.

## 4 RESULTS

A set of simulations were performed using Corcos model excitation with flow in the plate's lengthwise ($x$) direction. The velocity was varied over a range encompassing above and below coincidence conditions. Intensity fields and magnitudes were examined versus flow velocity. This study is divided into two parts: Section 4.1 contains plots of the input power to the plate versus flow velocity and Section 4.2 shows the evolution of the intensity field as the flow changes from low to high velocity (or high to low convective wavenumber). Injected power at frequencies corresponding to the resonances of the (1,1), (3,1), and (4,1) simply supported plate modes are shown. The modes resonate at 1394, 4675, and 7638 Hz, based on thin plate calculations.

### 4.1 Injected Power versus Convective Velocity

The abscissas of the input power plots in this section indicate the ratio of the plate bending wavenumber component in the flow direction normalized by the convective wavenumber of the flow. Lower values of this ratio indicate slower flow, while higher values indicate faster flow. Aerodynamic coincidence between the convective pressures and bending wavenumbers occurs at $k_x/k_c=1$. We denote conditions where $k_x/k_c<1$ as subsonic (high convective wavenumber, slow flow) and $k_x/k_c>1$ as supersonic (low convective wavenumber, fast flow).

As in Wallace's paper on radiation resistance [25] (related by reciprocity to the input power shown here), modes fall into behavioral groupings based on their modal indices: input power to odd-odd indexed modes differs from input power to even-even and even-odd modes. The power input at the (1,1) mode resonance frequency is shown in Figure 4. The input power rises with increasing flow velocity until roughly aerodynamic coincidence ($k_x/k_c=1$). For slow flows the excitation wavenumber is much larger than the structural wavenumber, so that nearly equal parts of the plate are forced with positive and negative phase at low velocities, thus inefficiently exciting the plate. At high speeds, the input power asymptotically approaches the value predicted for a fully correlated pressure field (shown with a red asterisk on the right side of the plot). For very high flow velocities, the excitation wavenumber tends toward zero, as is the case for fully correlated (i.e. plane wave) excitation of the plate.

The right side of Figure 4 shows the $x$ component of the wavenumber spectra of the (1,1) plate mode and the Corcos model in the flow direction for aerodynamic coincidence. Increasing the flow velocity would move the convective ridge (the peak in the excitation spectrum) to the left, while decreasing the flow velocity would move it to the right. The convective ridge indicates that most of the energy in the Corcos model is contained in wavenumbers corresponding to the flow's convective velocity. The plate mode's wavenumber spectrum is a measure of the wavenumber sensitivity of the mode. High values indicate that the mode accepts energy well at a given wavenumber, while low values indicate that the mode is not susceptible to excitation at that wavenumber. A mode couples most efficiently to a turbulent flow when the convective ridge is aligned with the peak in the mode's wavenumber spectrum (aerodynamic coincidence, which is the condition shown in the figure).

The power input at the (3,1) resonance frequency is shown in Figure 5. The input power at this frequency, again, increases with increasing flow velocity until coincidence. At supersonic conditions ($k_x>k_c$), the input power oscillates with increasing flow velocity until it eventually converges to a constant input power corresponding to plane wave (fully correlated) excitation. The reason for the oscillation in input power is easily observed in the wavenumber spectra shown in the right side of Figure 5. The trough in the input power that occurs just above coincidence occurs at a wavenumber ratio of 3.23. At this wavenumber ratio, the

convective ridge aligns with the dip to the left of the principle peak of the modal wavenumber spectrum. In other words, for a wavenumber ratio of 3.23 (where a local minimum of input power occurs) most of the energy in the excitation model is contained in wavenumbers to which the (3,1) plate mode (in the flow direction) is insensitive. Thus, at this wavenumber ratio, power must be input to other, non-resonant modes. These modes accept less power than at frequencies close to their resonance frequencies. The input power, therefore, shows a dip.

Above a wavenumber ratio of 3.23, the convective ridge is located over the leftmost plateau of the resonant mode's wavenumber sensitivity. This plateau has a lower magnitude than the main peak of the (3,1) mode spectrum. As such, the mode is less coupled to the flow for extremely fast flow velocities. This is reflected in the input power plot, where at high flow velocities, the input power approaches a lower value than at coincidence. A more intuitive explanation of this lower value may be made in physical (as opposed to wavenumber) space. At high flow velocities, the three velocity antinodes (peak response locations) of the (3,1) mode are forced by a pressure field of nearly uniform phase. As such, the middle third of the plate is effectively being forced 180 degree out of phase with the left and right thirds of the plate. At coincidence, however, the convective and structural wavenumbers are equal in the flow direction. Therefore, at coincidence, all three velocity antinodes are being forced in phase with each other by the pressure field, resulting in stronger coupling to the flow and greater input power. This phenomenon will be illustrated graphically in the next section.

Figure 6 shows the input power and wavenumber spectra at the (4,1) plate resonance frequency. They are included to show the difference between the coupling of odd-odd and even-odd modes to a TBL flow excitation. The input power at this frequency rises as the flow velocity increases toward coincidence and goes through a region of oscillation as $k_c$ becomes smaller than $k_x$. After the region of oscillation, the input power decreases steadily with increasing flow velocity, eventually reaching a steady value corresponding to the power input by a fully correlated wavefront. The decrease of input power with increasing velocity is explained by the (4,1) mode's wavenumber spectrum. Modes with even indices in the flow direction exhibit low wavenumber rolloff, unlike odd ordered modes. This is because, for even order modes, equal portions of the plate are being forced with positive and negative phase by a fully correlated wave front. As such, the contributions of the resonant mode and all other even indexed modes vanish for relatively high flow velocities. This leaves only the odd ordered (non-resonant) modes to contribute to the response (and the input power) of the plate. It has been shown for the (1,1) and (3,1) resonances that these modes have a finite, zero slope wavenumber sensitivity at low wavenumbers. Thus, as shown in Figure 6, the input power at the resonance frequencies for even ordered modes should approach a constant, albeit lower value than for the odd resonance frequencies at high flow velocities.

Several additional observations regarding input power versus flow velocity should be made. First, the number of peaks and nulls in the input power curve below its fully correlated limit should increase with increasing mode index in the flow direction. Specifically, the number of peaks in the input power curve are equal to the number of peaks in the resonant mode's flow-direction wavenumber spectrum below the primary wavenumber peak. Also, it should be noted that the input power (particularly for slow flows) will vary depending on the excitation model chosen. Recall that the Corcos TBL model used here tends to predict stronger content in the low wavenumber region than various other models [24]. As such, the input power predicted for slower flows in this paper is higher than that which would be predicted using other TBL models.

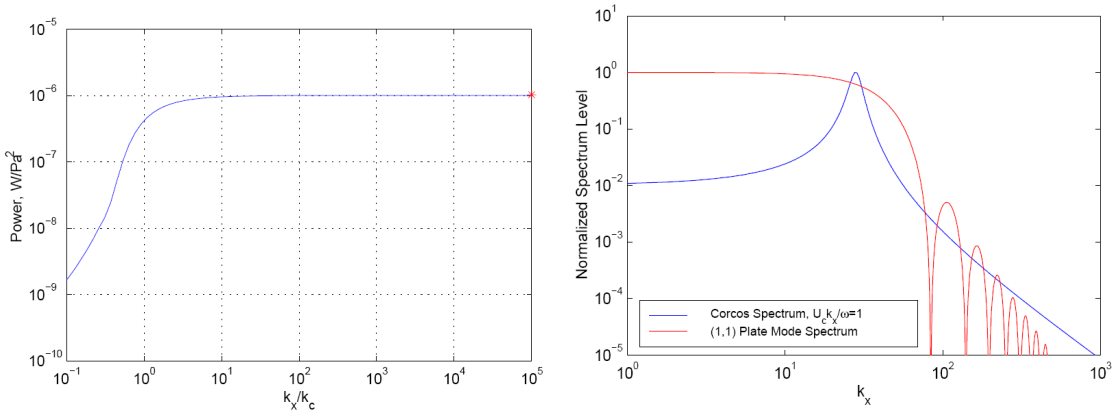


Figure 4: Left: simulated input power vs. structural/flow wavenumber ratio at (1,1) resonance frequency; the red asterisk to the right indicates the power input by a fully correlated pressure field. Right: wavenumber spectra of the (1,1) mode and Corcos TBL excitation at a flow speed where the convective and peak modal wavenumbers coincide.

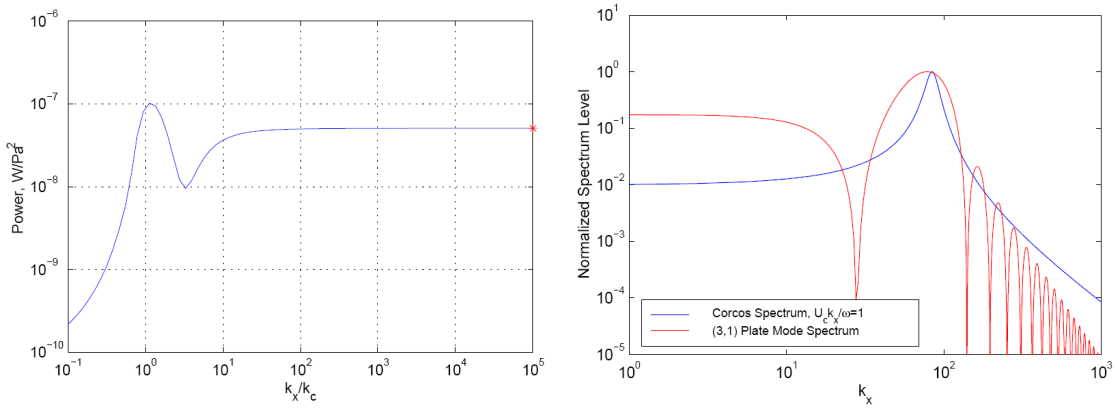


Figure 5: Left: simulated input power vs. structural/flow wavenumber ratio at (3,1) resonance frequency; the red asterisk to the right indicates the power input by a fully correlated pressure field. Right: wavenumber spectra of the (3,1) mode and Corcos TBL excitation at a flow speed where the convective and peak modal wavenumbers coincide.

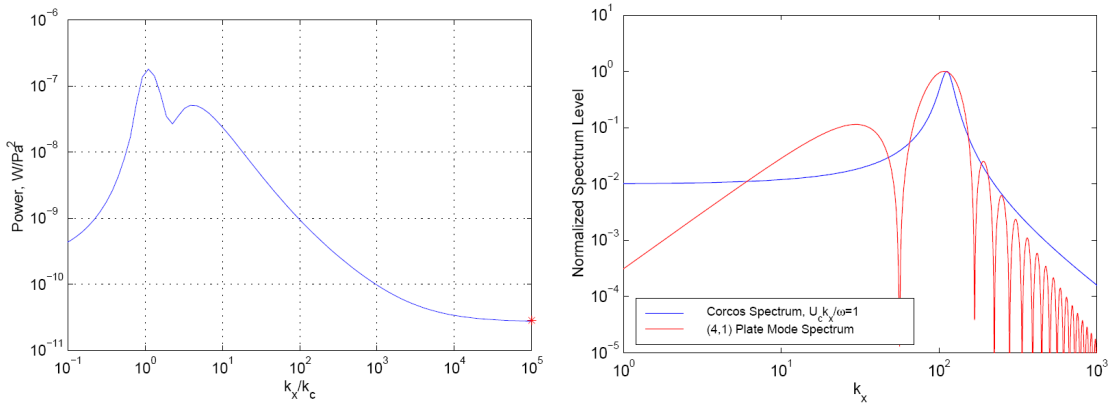


Figure 6: Left: simulated input power vs. structural/flow wavenumber ratio at (4,1) resonance frequency; the red asterisk to the right indicates the power input by a fully correlated pressure field. Right: wavenumber spectra of the (4,1) mode and Corcos TBL excitation at a flow speed where the convective and peak modal wavenumbers coincide.

### 4.2 Effects of Convective Velocity on SI Fields

Figure 7 and Figure 8 show intensity simulations at the (3,1) resonance frequency for flow speeds of 10 to 50% of the bending wave speed in the plate (subsonic conditions). The figures show (a) an example of the correlation of the TBL pressure field with a reference point at the plate center, (b) the structural intensity field, shown as a vector array superimposed over a contour of intensity magnitude, (c) the distribution of power input to the plate, and (d) the divergence of the intensity field. The three lobed mode shape pattern of the (3,1) mode is clearly visible in Figure 7, and has fewer oscillations over its length than the pressure excitation. The intensity field shows a broad vortex on the left side of the plate, with intensity converging to the damper in the upper right quadrant of the plate. The divergence plot clearly shows the location of the damper, and shows that power is injected over most of the plate.

Figure 9 shows a simulation at aerodynamic coincidence. The intensity magnitude scale reaches a maximum near this point, as seen in the input power curve in Figure 5. While the intensity amplitudes change, it is interesting to note that the intensity field patterns do not change significantly for $0.1 < k_x/k_c < 1.0$.

Figure 10 shows the simulated intensity field for supersonic conditions ($k_x/k_c = 10$). For high speed TBL flow excitation, the intensity field differs slightly from the subsonic conditions, with a null appearing between the large intensity vortex on the left, and the power travelling into the damper on the right. For subsonic flows, the circulation of energy on the left two thirds of the plate is coupled to the right third of the plate. For the fast flow cases the input power distribution shows power leaving the plate from its central third (the blue region in the input power plot). In these cases, the divergence plots show a distributed energy sink over this third as well (the orange region in the center). It appears that some of the energy entering the plate in the left third of the plate exits the plate in the central third. The energy entering the plate in the right third appears to exit the plate via the damper. For slower flows (Figures 7-9), the middle third of the plate is not excited out of phase with the outer thirds. As such, the energy from the left third does not exit the plate in the middle, and instead must be dissipated by either material losses or the damper. A simulation for a fully correlated excitation field is included for comparison purposes in Figure 11. The simulated intensity field for the fully correlated excitation is similar in shape and magnitude, as expected, to the Corcos excitation when the flow speed greatly exceeds the bending wavespeed in the plate.

## 5 SUMMARY AND CONCLUSIONS

Analytic simulations of the structural intensities and power flows of a TBL excited flat rectangular baffled simply supported brass plate are presented. The simulations use methods developed by the authors previously [19,20], and combine transfer functions between pressure loads and plate responses (displacement, rotation, moment, and shear) with cross-spectral density matrices of forcing functions. The power injected into the plate at frequencies corresponding to the resonances of several low order modes is shown. Power input peaks near convective flow velocities which coincide with the peak wavenumbers of the mode shapes, and converges to constant values at very high convective velocities. Structural intensity patterns are nearly constant for a wide range of flow velocities, only changing when flow velocities are very high, where the pressure loads over the plate become nearly perfectly correlated.

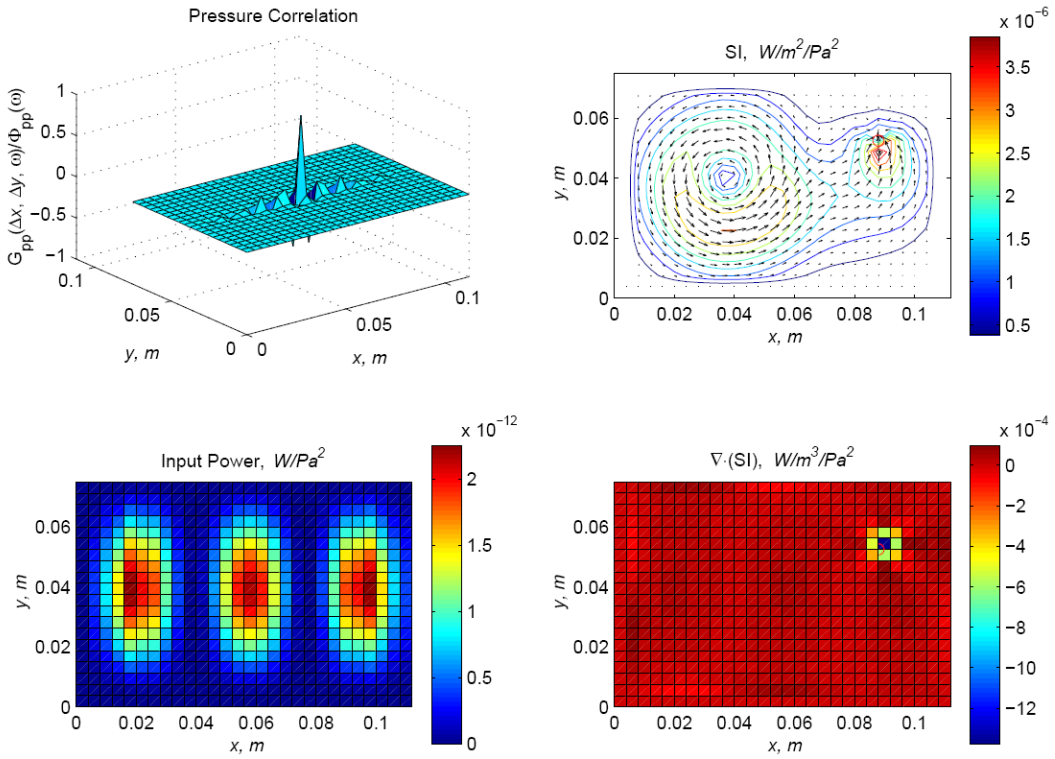


Figure 7: Simulated S-I (upper right), pressure correlation (upper left), distributed input power (lower left), and divergence (lower right) at (3,1) resonance frequency, $k_x/k_c$=0.1 (subsonic flow).

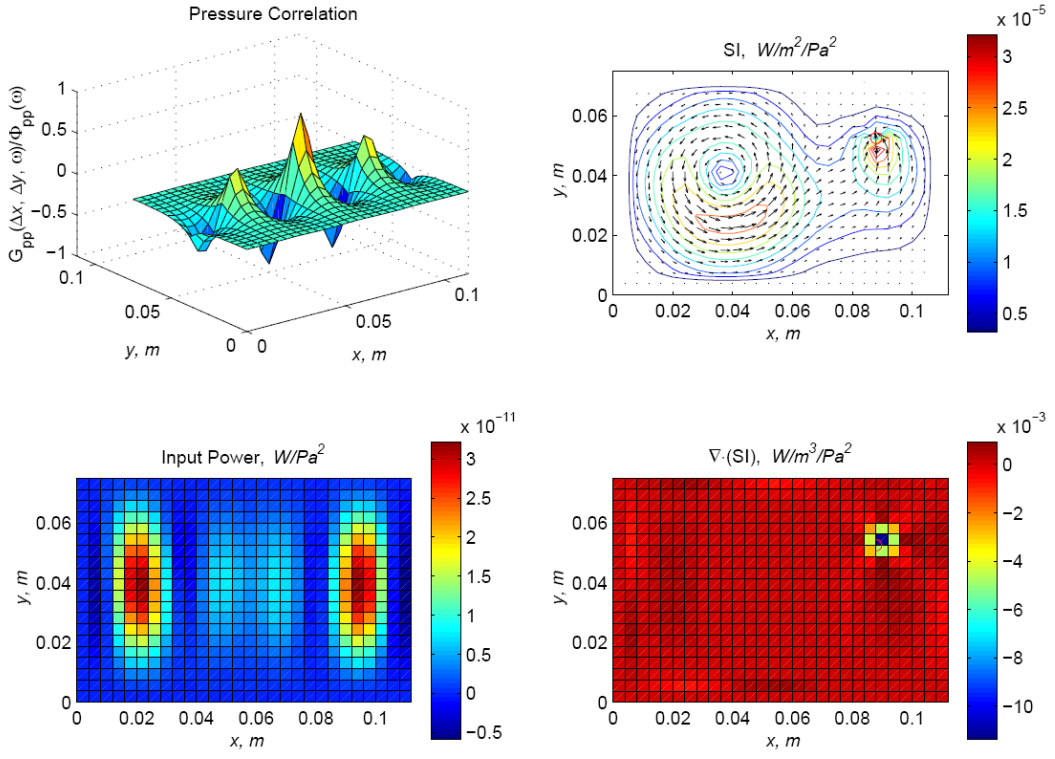


Figure 8: Simulated S-I (upper right), pressure correlation (upper left), distributed input power (lower left), and divergence (lower right) at (3,1) resonance frequency, $k_x/k_c$=0.5 (subsonic flow).

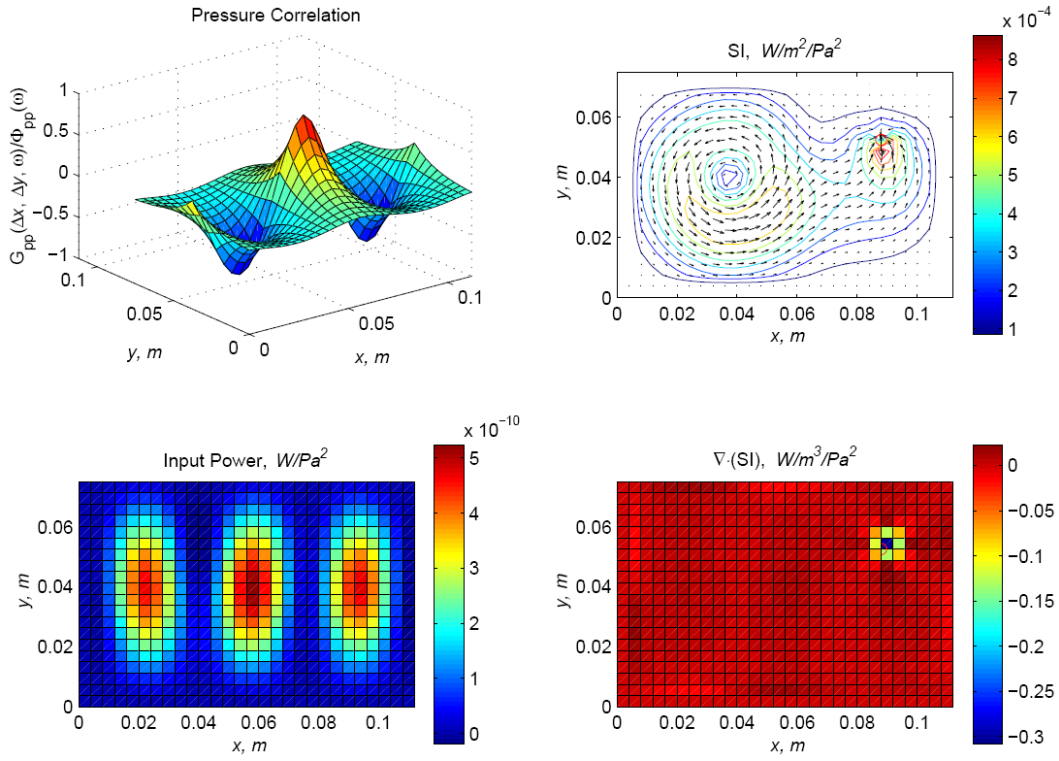


Figure 9: Simulated S-I (upper right), pressure correlation (upper left), distributed input power (lower left), and divergence (lower right) at (3,1) resonance frequency, $k_x/k_c$=1.0 (coincidence).

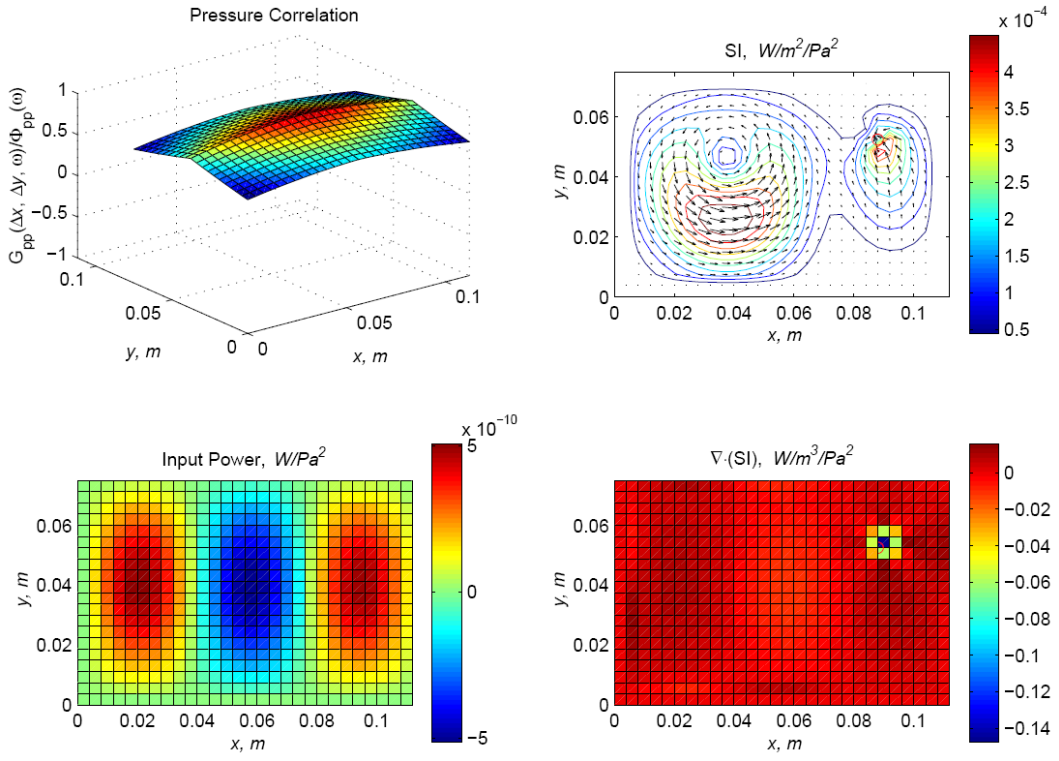


Figure 10: Simulated S-I (upper right), pressure correlation (upper left), distributed input power (lower left), and divergence (lower right) at (3,1) resonance frequency, $k_x/k_c$=10.0 (supersonic flow).

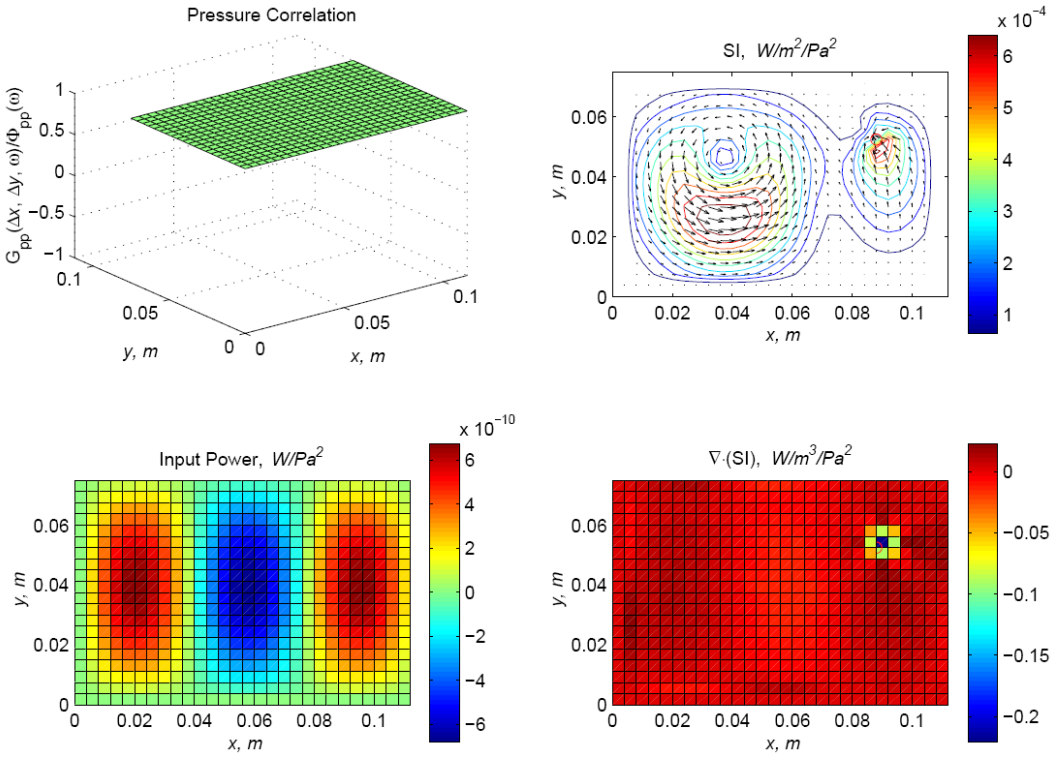


Figure 11: Simulated S-I (upper right), pressure correlation (upper left), distributed input power (lower left), and divergence (lower right) at (3,1) resonance frequency, fully correlated loading.

## REFERENCES


[1] D.U. Noiseaux, 1970, "Measurement of Power Flow in Uniform Beams and Plates," *J. Acoust. Soc. Amer.*, 47 (1, Part 2), 238-247.

[2] G. Pavic, 1976, "Measurement of Structure-Borne Wave Intensity, Part 1: Formulation of the Methods," *J. Sound and Vib.*, 49, 221-230.

[3] S.A. Hambric, 1990, "Power Flow and Mechanical Intensity Calculations in Structural Finite Element Analysis," *ASME J. Vib. and Ac.*, 112 (4), 542-549.

[4] L. Gavric and G. Pavic, 1993, "A Finite Element Method for Computation of Structural Intensity by the Normal Mode Approach," *J. Sound and Vib.*, 164 (1), 29-43.

[5] S.A. Hambric and P.D. Taylor, 1994, "Comparison of Experimental and Finite Element Structure-Borne Flexural Power Measurements for a Straight Beam," *J. Sound and Vib.*, 170 (5), 595-605.

[6] R.P. Szwerc, C.B. Burroughs, S.A. Hambric, and T.E. McDevitt, 2000, "Power Flow in Coupled Bending and Longitudinal Waves in Beams," *J. Acoust. Soc. Amer.*, 107 (6), 3186-3195.

[7] S.A. Hambric, J.M. Cuschieri, C.R. Halkyard, B.R. Mace, and R.P. Szwerc, 2002, "Low-frequency Measurements and Predictions of the Structural-Acoustic Properties of the INCE standard T-beam Structure," *Noise Control Eng. J.*, 50 (3), 90-99.

[8] X.D. Xu, H.P. Lee, and C.Lu, 2005, “Power Flow Paths in Stiffened Plates,” *J. Sound and Vib.*, 282, 1264-1272.

[9] J.R.F. Arruda and P. Mas, 1996, “Predicting and Measuring Flexural Power Flow in Plates," *Proc. of SPIE*, Vol. 2868, Washington D.C., 149-163.

[10] A. Powell, 1958, “On the fatigue failure of structures due to vibrations excited by random pressure fields,” *J. Acoust. Soc. Amer.*, 30 (12), 1130-1135.

[11] L. Maestrello, 1965, “Measurement of noise radiated by boundary layer excited panels,” *J. Sound and Vib.*,, 2 (2), 100-115.

[12] J.F. Wilby, 1967, “The response of simple panels to turbulent boundary layer excitation,” Technical Report AFFDL-TR-67-70.

[13] L.D. Jacobs, D.R. Lagerquist, and F.L. Gloyna, 1970, “Response of complex structures to turbulent boundary layers,” *Journal of Aircraft*, 7 (3), 210-219.

[14] W.J. Chyu, and M.K. Au-Yang, 1972, “Random response of rectangular panels to the pressure field beneath a turbulent boundary layer in subsonic flows,” NASA Technical Note D-6970.

[15] M.K. Au-Yang, 1975, “Response of Reactor Internals to Fluctuating Pressure Forces,” *Nuclear Eng. and Des.*, 35, 361-375.

[16] M.K. Au-Yang and W.H. Connelly, 1977, “A Computerized Method for Flow-Induced Random Vibration Analysis of Nuclear Reactor Internals,” *Nuclear Eng. and Des.*. 42, 257-263.

[17] S.A. Hambric, Y.F. Hwang, and W.K. Bonness, 2004, “Vibrations of Plates with Clamped and Free Edges Excited by Low-Speed Turbulent Boundary Layer Flow,” *Journal of Fluids and Structures*, 19, 93-110.

[18] S.A. Hambric, M.L. Jonson, J.B. Fahnline, and R.L. Campbell, 2005, “Simulating the Vibro-Acoustic Power of Fluid-Loaded Structures Excited by Randomly Distributed Fluctuating Forces,” *Proceedings of NOVEM 2005*, St. Raphael, France.

[19] Daley, M.J., and Hambric, S.A., February 2009, “A Method to Simulate Structural Intensity Fields in Plates and General Structures Induced by Spatially and Temporally Random Excitation Fields," *ASME J. Vib. and Ac.*, 131.

[20] M.J. Daley and S.A. Hambric, 2005, “Simulating and Measuring Structural Intensity Fields in Plates Induced by Spatially and Temporally Random Excitation,” *ASME J. Vib. and Ac.*, 127, 451-457.

[21] J.W. Verheij, 1980, “Cross Spectral Density Methods for Measuring Structure Borne Power Flow on Beams and Pipes,” *J. Sound and Vib.*, 70 (1), 133-139.

[22] J. Linjama, and T. Lahti, 1992, “Estimation of Bending Wave Intensity in Beams Using the Frequency Response Technique,” *J. Sound and Vib.*, 153 (1), 21-36.

[23] Corcos, G.M., 1963, “Resolution of pressure in turbulence,” *J. Acoustic. Soc. Amer.*, 35, 2, 192-199.

[24] Hwang, Y, Bonness, W, and Hambric, S, 2009, “Comparison of semi-empirical models for turbulent boundary layer wall pressure spectra,” *J. Sound and Vib.*, 319, 199-217.

[25] Wallace, C.E., 1972, “Radiation Resistance of a Rectangular Panel, ” *J. Acoust. Soc. Amer.*, 51 (3, part 2), 946-952.